

## MCS MOTION: THE ROLE OF VERTICAL MOMENTUM TRANSPORT

Kelly M. Mahoney<sup>+</sup> and Gary M. Lackmann  
*North Carolina State University, Raleigh, North Carolina*

### 1. INTRODUCTION

Forecasting the motion of mesoscale convective systems (MCSs) remains a challenge to both human forecasters and numerical models. MCS movement is often the combined result of several physical processes that occur on different temporal and spatial scales, thus accurately predicting it is a complex problem. The redistribution of momentum within MCSs has been examined by previous studies, but few have focused on the downward branch of momentum transport in MCSs, and the ways in which both convective- and mesoscale downdrafts may affect the lower-tropospheric wind field. If such transports substantially alter the low-level momentum field, it is conceivable that MCS speed may be affected, either by the advective effect of increasing the mean cloud-bearing wind, or the propagative effect of increasing winds within the cold pool itself. Therefore, this study seeks to investigate the following question: What influence does the vertical momentum transport (of both large-scale and perturbation winds) by an MCS have on the ground speed of the MCS itself?

Although convective momentum transport (CMT) is not typically listed among the major processes by which MCSs translate through their surrounding environments (e.g., Fritsch and Forbes 2001; Houze 2004), the process in general has been examined in both observational and modeling studies. Most of these past studies have focused on the large-scale momentum field of the surrounding environment, or its parameterization in large-scale numerical models (e.g., Houze 1973; Grubišić and Moncrieff 2000; Mechem et al. 2006), while a few others have mentioned the potential importance of momentum transport as a key determinant of surface wind speed (e.g., Johns and Doswell 1992; Geerts 2001).

It is conceivable that CMT may impact MCS motion in two possible ways: (i) via the enhancement of the advective component of MCS motion due to the forward penetration of elevated portions of the rear inflow jet (RIJ), and/or (ii) an increase in system speed as downward CMT increases the speed of the cold pool itself (by increasing the speed of the winds within it). Each possibility is analyzed in section 3.

### 2. METHODOLOGY

#### *a) Model set-up*

In order to investigate the CMT process in a numerically-simulated MCS, the Weather Research and Forecasting (WRF; Skamarock et al. 2007) model is used in a way that employs a combination of real-case and idealized modeling techniques. This “quasi-idealized” combination uses simplified initial and boundary conditions within a real-case modeling framework; it includes a background baroclinic environment (an element largely neglected by many purely-idealized modeling studies of the past), which allows a more realistic treatment of the larger-scale environment by including an upper-level jet stream that is in thermal wind balance. The Coriolis force is also accounted for, which is important to MCS motion over extended time intervals.

Initial conditions for the simulation are generated using empirical relationships to produce a simple westerly jet stream in an environment with CAPE and a horizontal wind field in thermal wind balance. Thus, in order to produce a jet stream in thermal wind balance, the entire initial sounding (Fig. 1) is first uniformly nudged to be cooler (warmer) as latitude increases (decreases); in this way, the initial conditions more realistically represent the baroclinic background environment common to midlatitude MCSs (relative to more idealized studies in which a single uniform initial sounding is often used).

The convection is triggered by a 2°C warm bubble with horizontal dimensions 4km x 1km, located

---

<sup>+</sup> *Corresponding author address:* Kelly M. Mahoney, North Carolina State University, Dept. of Marine, Earth and Atmospheric Sciences, Raleigh, NC 27695. E-mail: kmmahon2@ncsu.edu

between the surface and 3 km. An inner domain with 1-km horizontal grid spacing (676 km x 604 km) lies within an outer domain of 4-km grid spacing (1800 km x 1800 km). Neither domain utilizes a cumulus parameterization (CP) scheme, but both employ the Yonsei University (YSU) planetary boundary layer (PBL) scheme (Hong et al. 2006). Model simulation times are hereafter denoted by “forecast time” FHH or FHH:mm, specifying the number of hours (HH) and minutes (mm) into the simulation. Further details of both this approach and model setup are given in Mahoney et al. (2009).

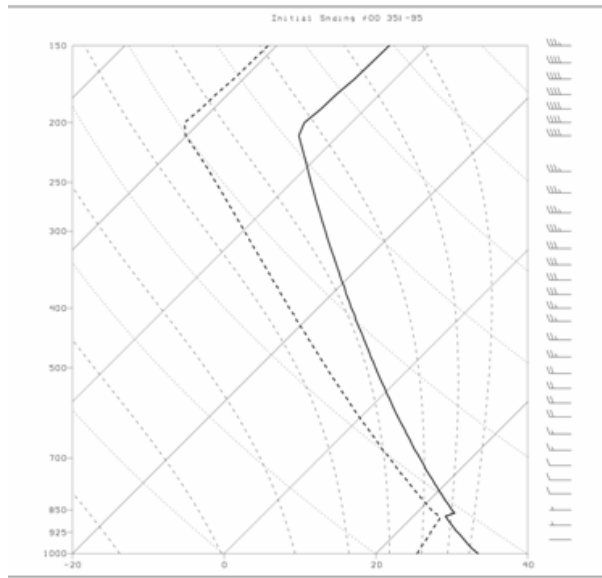


Figure 1. Initial sounding shape used to initialize the quasi-idealized MCS simulation (at (35°lat; -95°lon)). Temperature (°C, solid line), dewpoint (°C, dashed line), wind barbs in knots at right.

### b) Momentum budgets

Momentum budgets are computed for the simulated MCS from both an Eulerian and Lagrangian framework, according to (1) and (2), respectively.

$$\frac{\partial u}{\partial t} + c_x \frac{\partial u}{\partial x} + c_y \frac{\partial u}{\partial y} = \underbrace{-(u - c_x) \frac{\partial u}{\partial x}}_{TEN_x} - \underbrace{(v - c_y) \frac{\partial u}{\partial y}}_{HAu_x} - \underbrace{w \frac{\partial u'}{\partial z}}_{HAu_y} - \underbrace{w \frac{\partial \bar{u}}{\partial z}}_{VAu'} - \underbrace{fv}_{VA\bar{u}} - \frac{1}{\rho} \frac{\partial p}{\partial x} + R_x \quad (1)$$

$$\frac{d\vec{V}}{dt} = -\frac{1}{\rho} \nabla p - f\vec{k} \times \vec{V} + R \quad (2)$$

Budget equations, term definitions, and computational details are described more fully in Mahoney et al. (2009).

## 3. RESULTS

The simulated MCS organizes into a quasi-linear, bowing MCS that exhibits an intense leading convective line followed by a smaller region of lighter precipitation, generally reflecting the classic “leading convective-trailing stratiform” MCS structure (Fig. 2) (e.g., Houze et al. 1990).

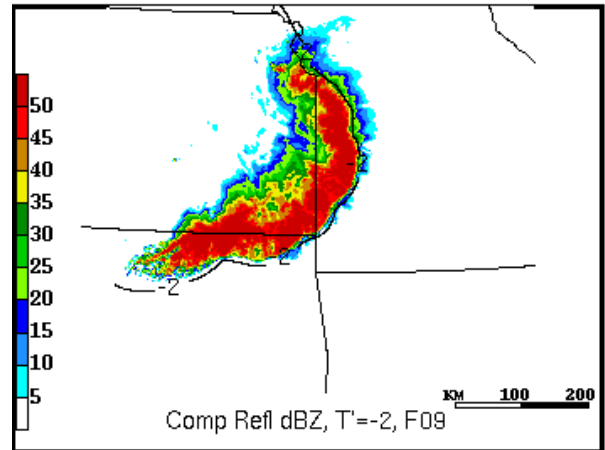


Figure 2. Simulated composite reflectivity (dBZ, shaded as indicated at right) and cold pool outline ( $T'=-2^\circ\text{C}$  at 0 m (black, solid)) at F09.

### a) MCS Motion

In order to understand the nature of the simulated MCS motion, the evolution of the MCS and its cold pool from developing to mature stages are analyzed.

After 3 - 4 hours into the simulation, the average cold pool depth is ~1.5 km, and the maximum temperature perturbation generally approaches -10°C at the surface and averages -6°C through its depth; such values are consistent with those found by previous observational and modeling studies (e.g., Engerer et al. 2008). The speed at which the cold pool moves can be calculated by its theoretical density current speed,  $c$ . Despite the strong sensitivity of buoyancy-based cold pool calculations to relatively small thermal and pressure perturbations, we wish to establish an estimate of theoretical cold pool speed here; details of the specific calculation are described in Mahoney et al. (2009). The theoretical cold pool speed is shown in Fig. 3. Differences between the theoretical and observed cold pool speeds, particularly during periods of MCS acceleration (discussed below),

indicate that the winds in the cold pool are not simply a product of the static pressure field produced by the cold pool.

The advective component of MCS motion is often estimated by measuring the mean wind in the cloud-bearing layer (e.g., Corfidi et al. 1996); the dotted line in Fig. 3 shows the evolution of this field over time. The translational speed of the system is illustrated by the solid line in Fig. 3 and shows that the system speed accelerates from about  $6 \text{ ms}^{-1}$  to  $22 \text{ ms}^{-1}$  from the MCS's initial to mature stages. The dashed line in Fig. 3 shows the average value of the maximum windspeed found over the lowest 3 km of each grid column in the leading 40 km of the cold pool (a volume over which additional quantities are averaged in the following section).

MCS speed and the average maximum wind speed in the leading portion of the cold pool are relatively closely matched, and the evolution of each field with time is also similar (the two quantities have a correlation coefficient of 0.9 and a root-mean-square error of  $2 \text{ ms}^{-1}$ ). Thus, the MCS largely moves at the speed of the winds in the leading edge of its cold pool, which is likewise the speed at which the actual cold pool and gust front move (e.g., Goff 1976; Lafore and Moncrieff 1989). Furthermore, comparing the calculated theoretical cold pool speed to the actual cold pool speed reveals that the theoretical value not only underestimates (overestimates) the actual value at mature (initial) stages, but also fails to fully explain the period of maximum acceleration from F05 – F07; this suggests that the speed of the cold pool is not driven and/or maintained by density current mechanics alone.

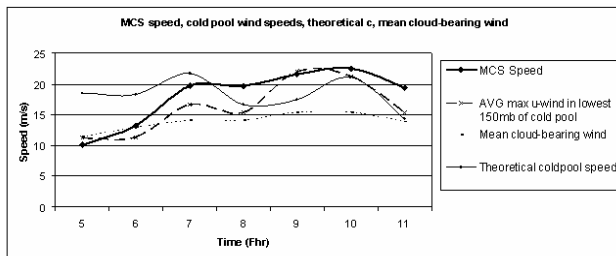


Figure 3. Speed of MCS ( $\text{ms}^{-1}$ , solid), average of grid point maximum wind speed in the lowest 3 km of the cold pool ( $\text{ms}^{-1}$ , large dashed), average mean cloud-bearing wind (from 900 – 200 hPa,  $\text{ms}^{-1}$ , small dashed), and theoretical cold pool speed  $c$  ( $\text{ms}^{-1}$ , thin solid).

#### b) Convective momentum transport

Two momentum budgets are computed using WRF model output in order to (i) determine which terms in the momentum equation contribute most to the enhanced wind speeds in the leading portion of the cold pool, and (ii) quantify the role of CMT in the MCS momentum field (and hence its forward motion). Thus, we investigate the possibility that contribution from CMT may at least partially explain the discrepancy between the observed cold pool speed of the simulated system and the theoretical cold pool speed calculated above.

The Eulerian budget terms are averaged in two system-relative volumes (illustrated by the outlined boxes in Fig. 4); one at the leading edge of the cold pool ( $\text{VOL}_{\text{leading}}$ , Fig. 4a) and the other toward the middle-to-rear portion of the system ( $\text{VOL}_{\text{trailing}}$ , Fig. 4d). The volumes are laterally bounded to the north and south to encompass the portion of the system that moves most nearly zonally, and the east-to-west extent is limited to 0 – 40km (40 – 120km) behind the leading edge of the cold pool for  $\text{VOL}_{\text{leading}}$  ( $\text{VOL}_{\text{trailing}}$ ). Defining the volumes to include lower-to-mid levels following the leading edge of the system (0 – 3 km and 0 – 6 km for  $\text{VOL}_{\text{leading}}$  and  $\text{VOL}_{\text{trailing}}$ , respectively) serves to focus on the low-level storm outflow contained within the cold pool and also on the rear-to-front flow branch, which contributes to changes in low-level westerly momentum.

Figure 4 reveals a positive contribution from the vertical advection of perturbation rear-to-front flow ( $VAu'$ ) in  $\text{VOL}_{\text{leading}}$  at both developing and mature stages (Figs 4b,e), confirming that the process is of first-order importance in strengthening westerly flow in the forward part of the storm. In  $\text{VOL}_{\text{leading}}$ ,  $VAu'$  averages  $\sim 13 \text{ m s}^{-1}\text{h}^{-1}$  throughout the simulation, clearly contributing to the acceleration of the system.

$\text{VOL}_{\text{trailing}}$  is used to diagnose the role of the budget terms in the generally westerly momentum field produced in the RIJ region. Within the trailing volume, the vertical advection of the background wind ( $VA\bar{u}$ ) and the pressure gradient acceleration in the east-west direction ( $PGA_x$ ) contribute to the local acceleration of the RIJ (Fig.4c,f). The

volume-averaging approach clearly illustrates that in  $VOL_{trailing}$  there is a relatively modest but significant contribution from both the  $PGA_x$  term and the  $VA\bar{u}$  term, as they each supply a steady acceleration of  $2 - 8 \text{ ms}^{-1}\text{h}^{-1}$  to the rear-to-front flow in the trailing stratiform portion of the system. From an Eulerian perspective, it is difficult to comment on how these terms contribute specifically to storm motion, given that the overall effect is likely integrated along the sloping RIJ descent. Therefore, the advection terms can be eliminated and by instead moving *with* the descending parcels, a Lagrangian budget is calculated to more fully understand (i) the local acceleration of the RIJ, (ii) the extent to which  $PGA$  impacts MCS motion, and (iii) the connection between the leading and trailing volumes used above.

The Lagrangian budget computes parcel acceleration, pressure gradient acceleration, and Coriolis terms along parcel trajectories, according to (2). A composite of 50 trajectories that originate in the RIJ reveal that the average parcel motion sampled is one of descent from mid-levels into the cold pool (to within approximately 100 m of the surface) by F11. Along this trajectory, there is a marked period of maximized acceleration, from F07:00 to F08:25 (*not shown*), during which a strong pressure gradient acceleration exists in the direction of parcel motion. Over this 85-min time interval, the pressure gradient acceleration accounts for an acceleration of  $\sim 8.5 \text{ ms}^{-1}$  (its average value  $\sim 6 \text{ ms}^{-1}\text{h}^{-1}$ ), and the composite trajectory's average wind speed indeed strengthens by  $\sim 9.5 \text{ ms}^{-1}$  (*not shown*). Because the pressure gradient acceleration term is the only means by which the MCS momentum field may accelerate or decelerate along a parcel trajectory, the role of the mid-level mesolow and resulting pressure gradient acceleration in the CMT process is more clearly defined.

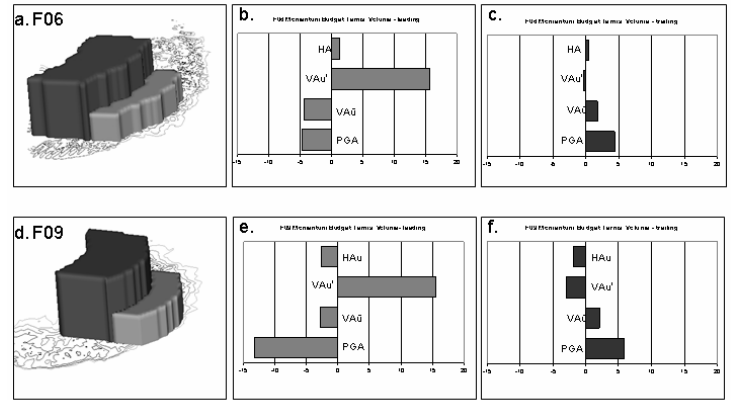


Figure 4. a)  $VOL_{leading}$  (light gray) and  $VOL_{trailing}$  (dark gray) at F06, b) momentum budget term averages as labeled over  $VOL_{leading}$  at F06 in  $\text{ms}^{-1}\text{h}^{-1}$ , c) as in b) but for  $VOL_{trailing}$ , d) as in a) but for F09, e) as in b) but for F09, f) as in c) but for F09.

### c) CMT and severe surface wind potential

The Lagrangian budget also illustrates the critical role of downward CMT in bringing the accelerated RIJ flow surface-ward. The parcels experience more than half of their acceleration (nearly  $7 \text{ ms}^{-1}$ ) prior to the steep descent toward the surface, indicating that vertical advection (i.e., CMT) is a key process by which near-surface wind speeds (as well as MCS speed) increase. The average trajectory path also reveals a direct connection between the RIJ and the cold pool as suggested by many past studies (e.g., Zipser 1977; Smull and Houze 1987; Lafore and Moncrieff 1989), and that in many places near the leading portion of the system, the RIJ indeed descends to the surface (or closely above). This detail may hold important implications for wind speeds experienced at the earth's surface. (e.g., Johns and Doswell 1992; Weisman 1992; Geerts 2001).

Several recent studies have found that strong surface winds are often produced when mesovortices along the leading edge of the convective line and a descending RIJ are co-located (e.g., Trapp and Weisman 2003; Wakimoto et al. 2006; Atkins and St. Laurent 2008). This mechanism appears to occur at several times and locations in this simulation as well, and the CMT process is found to be linked to these areas of severe surface winds (*not shown*). Further analysis of the

role of CMT in determining surface convective wind gusts is ongoing.

#### 4. SYNTHESIS AND CONCLUSIONS

This study demonstrates that the motion of a numerically-simulated MCS is significantly impacted by convective momentum transport. Momentum budgets computed from both a Lagrangian and an Eulerian perspective reveal that the vertical advection of the perturbation wind contributes largely to the momentum field at the leading edge of the cold pool -- the region in which the resulting accelerated winds drive system motion. The momentum budgets also illustrate that the pressure gradient acceleration and the vertical advection of the background environmental wind contribute to the acceleration of rear-to-front momentum in the middle- to rearward portions of the storm. This contribution both generates and later reinforces the perturbation flow transports into the cold pool, and thus accelerates the MCS. These processes are schematized in Fig. 5.

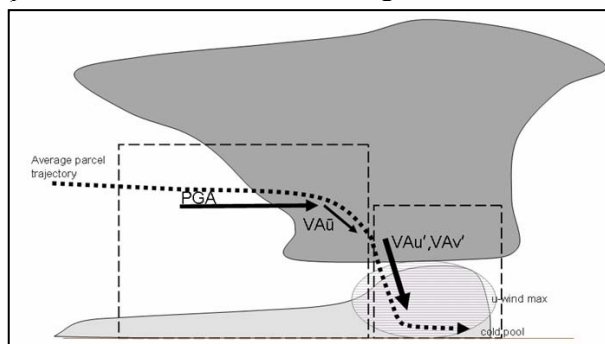


Figure 5. Schematic of relative contributions of momentum budget terms PGA and vertical advection (VA) processes to CMT as indicated by black arrows (thickness of arrows an approximate indication of relative magnitude of terms, and dashed boxes show general locations of  $VOL_{leading}$  and  $VOL_{trailing}$ ).

Results from both the Eulerian and Lagrangian momentum budgets indicate a significant contribution to MCS speed from CMT: system acceleration during times of large downward transport suggest that an increase of system speed on the order of  $5 - 10 \text{ ms}^{-1}$  over a period of 3 - 4 hours may be largely due to CMT.

These results also suggest that the omission of the CMT process in many operational NWP model CP schemes is questionable, and may contribute to a

negative bias in numerical forecasts of MCS motion at grid lengths where CP schemes are needed (Mahoney and Lackmann 2007). It is possible that current “manual” MCS motion forecast methods [e.g., Corfidi vectors (Corfidi et al. 1996)] may also benefit from a more precise inclusion of the CMT processes as described here. Finally, the CMT process may be of importance to severe weather forecasting: downward CMT in MCSs likely contributes to severe surface winds and downbursts (e.g., Vescio and Johnson 1992; Weisman 1992; Geerts 2001). The specific implications of this relationship and how it differs from classic severe wind generation mechanisms such as thermodynamically-driven microbursts are being investigated further as ongoing work.

Additional analysis is also underway to examine the role of the trailing stratiform region in determining the relative importance of CMT in various types of storms and storm environments. Further incorporating CMT into the MCS forecast process is also desirable, both by improving its representation in existing CP schemes and also by more completely integrating CMT into conceptual models of MCS motion.

#### 5. ACKNOWLEDGEMENTS

Support for this research was provided by National Science Foundation Grant ATM-0603760, awarded to North Carolina State University. We wish to acknowledge Drs. Matthew Parker, Sandra Yuter, Anantha Aiyyer, Morris Weisman, Stan Trier, Jack Kain, and Mike Coniglio for helpful insights and discussions concerning this research. The authors would also like to thank NCAR and the National Science Foundation for the availability of the WRF model.

#### 6. REFERENCES

- Atkins, N. T., and M. St. Laurent, 2008: Bow echo mesovortices. Part I: Processes that influence their damaging potential. *Mon. Wea. Rev.*, In Press
- Bluestein, H. R., 1993: *Synoptic-Dynamic Meteorology in Midlatitudes. Vol. II: Observations and Theory of Weather Systems*. Oxford University Press, 594 pp.

- Corfidi, S. F., J. H. Meritt and J. M. Fritsch, 1996: Predicting the movement of mesoscale convective complexes. *Wea. Forecasting*, **11**, 41–46.
- Engerer, N. A., D. J. Stensrud, and M. C. Coniglio, 2008: Surface characteristics of observed cold pools. *Mon. Wea. Rev.*, **136**, 4839–4849.
- Fritsch, J. M., and G. S. Forbes, 2001: Mesoscale convective systems. Severe Convective Storms, Meteor. Monogr., No. 50, Amer. Meteor. Soc., 323–357.
- Geerts, B., 2001: Estimating downburst-related maximum surface wind speeds by means of proximity soundings in New South Wales, Australia. *Wea. Forecasting*, **16**, 261–269.
- Goff, C. R., 1976: Vertical structure of thunderstorm outflows. *Mon. Wea. Rev.*, **104**, 1429–1440.
- Grubišić, V., and M. W. Moncrieff, 2000: Parameterization of convective momentum transport in highly baroclinic conditions. *J. Atmos. Sci.*, **57**, 3035–3049.
- Hong, S. Y., Y. Noh, and J. Dudhia, 2006: A new vertical diffusion package with an explicit treatment of entrainment processes. *Mon. Wea. Rev.*, **134**, 2318–2341.
- Houze, R. A., Jr., 1973: A climatological study of vertical transports by cumulus-scale convection. *J. Atmos. Sci.*, **30**, 1112–1123.
- , 2004: Mesoscale convective systems. *Rev. Geophys.*, **42**, 10.1029/2004RG000150, 43 pp.
- , B. F. Smull, and P. Dodge, 1990: Mesoscale organization of springtime rainstorms in Oklahoma. *Mon. Wea. Rev.*, **118**, 613–654.
- Johns, R. H., and C. A. Doswell, 1992: Severe local storms forecasting. *Wea. Forecasting*, **7**, 588–612.
- Lafore, J. P., and M. W. Moncrieff, 1989: A numerical investigation of the organization and interaction of the convective and stratiform regions of tropical squall lines. *J. Atmos. Sci.*, **46**, 521–544.
- Mahoney, K. M., and G. M. Lackmann, 2007: The effect of upstream convection on downstream precipitation. *Wea. Forecasting*, **22**, 255–277.
- , ———, Parker, M. D., 2009: The role of momentum transport in the motion of a quasi-idealized mesoscale convective system. *Mon. Wea. Rev.*, In Press
- Mechem, D. B., S. S. Chen, and R. A. Houze, Jr., 2006: Momentum transport processes in the stratiform regions of mesoscale convective systems over the western Pacific warm pool. *Quart. J. Roy. Meteor. Soc.*, **132**, 709–736.
- Skamarock, W. C., M. L. Weisman, and J. B. Klemp, 1994: Three-dimensional evolution of simulated long-lived squall lines. *J. Atmos. Sci.*, **51**, 2563–2584.
- Smull, B. F., and R. A. Houze, Jr., 1987: Rear inflow in squall lines with trailing stratiform precipitation. *Mon. Wea. Rev.*, **115**, 2869–2889.
- Trapp, R. J., and M. L. Weisman, 2003: Low-Level Mesovortices within Squall Lines and Bow Echoes. Part II: Their Genesis and Implications. *Mon. Wea. Rev.*, **131**, 2804–2823.
- Vescio, M. D., and R. H. Johnson, 1992: The surface-wind response to transient mesoscale pressure fields associated with squall lines. *Mon. Wea. Rev.*, **120**, 1837–1850.
- Wakimoto, R. M., H. V. Murphey, C. A. Davis, and N. T. Atkins, 2006: High winds generated by bow echoes. Part II: The relationship between the mesovortices and damaging straight-line winds. *Mon. Wea. Rev.*, **134**, 2813–2829.
- Weisman, M. L., 1992: The role of convectively generated rear-inflow jets in the evolution of long-lived mesoconvective systems. *J. Atmos. Sci.*, **49**, 1826–1847.
- Zipser, E., 1977: Mesoscale and convective-scale downdrafts as distinct components of squall-line structure. *Mon. Wea. Rev.*, **105**, 1568–1589.